

## Similarity transformed semiclassical dynamics

Troy Van Voorhis<sup>a)</sup> and Eric J. Heller

*Department of Chemistry and Chemical Biology and Department of Physics, Harvard University, Cambridge, Massachusetts 02138*

(Received 7 August 2003; accepted 25 September 2003)

In this article, we employ a recently discovered criterion for selecting important contributions to the semiclassical coherent state propagator [T. Van Voorhis and E. J. Heller, *Phys. Rev. A* **66**, 050501 (2002)] to study the dynamics of many dimensional problems. We show that the dynamics are governed by a similarity transformed version of the standard classical Hamiltonian. In this light, our selection criterion amounts to using trajectories generated with the untransformed Hamiltonian as approximate initial conditions for the transformed boundary value problem. We apply the new selection scheme to some multidimensional Henon–Heiles problems and compare our results to those obtained with the more sophisticated Herman–Kluk approach. We find that the present technique gives near-quantitative agreement with the standard results, but that the amount of computational effort is less than Herman–Kluk requires even when sophisticated integral smoothing techniques are employed in the latter. © 2003 American Institute of Physics.

[DOI: 10.1063/1.1626621]

### I. INTRODUCTION

Coherent states are useful tools for a wide variety of systems.<sup>1</sup> For chemical problems in particular, there has been a long history of applications of harmonic oscillator coherent states (also known as Gaussian wave packets) for approximate quantum dynamics. Initially, the motivation for using Gaussian wave packets was that if the spread of the wave packet is small enough the effective potential always looks locally quadratic, in which case the particle never “sees” the anharmonic terms and the wave packet picture is physically justified.<sup>2</sup> Further, wave packets showed the potential for “smoothing over” the caustic singularities normally present for semiclassical approaches involving position or momentum eigenstates.<sup>3</sup> Thus, an intimate connection between coherent states and semiclassical dynamics was established early on.<sup>4</sup> It was later realized that a *swarm* of Gaussian wave packets might be useful as a time dependent basis, even in cases where the spreading of the wave function is quite large.<sup>5</sup> This idea was advanced further when Herman and Kluk showed that with the proper weight factors a swarm of Gaussian wave packets could be used to represent the wave function in a way that is exact in the semiclassical limit ( $\hbar \rightarrow 0$ ).<sup>6</sup> It turns out that this approximation is actually a *uniform* semiclassical approximation that is also part of a family of related integral expressions for the semiclassical propagator.<sup>7</sup> These techniques have been applied to a wide variety of problems in chemical dynamics, with an encouraging level of accuracy.<sup>8,9</sup> However, despite recent attempts at a “semiclassically exact” derivation,<sup>10</sup> this set of approximations is primarily viewed as an ansatz: a set of practical, useful, yet somewhat heuristic prescriptions for approximating quantum dynamics.

Meanwhile, there have been parallel developments based on the rigorous stationary path approximation to the quantum propagator in the coherent state basis. The first work in this direction was put forth by Klauder<sup>11</sup> who noted that in order to solve the required double-ended boundary conditions, one needed to effectively consider *two* sets of classical variables—one for the bra state and one for the ket. Subsequent work elucidated the importance of fluctuations about the classical path<sup>12</sup> and the presence of an “extra phase” in the semiclassical expression.<sup>13</sup> More recently, there has been a significant amount of work done to investigate the physical structure of the semiclassical coherent state propagator for small one-dimensional systems where the quantum dynamics is well understood.<sup>14–20</sup> However, until recently, this latter class of methods could generally be characterized as a rigorous and interesting but essentially impractical set of approximations.

The difficulty in applying the more rigorous form of the semiclassical coherent state propagator is that, for a many dimensional system, it is very difficult to locate trajectories that satisfy the double-ended boundary conditions. We have recently proposed a solution to this problem<sup>21</sup> that involves running the initial conditions forward in time and looking for times where the trajectory approaches the desired final point. The classical trajectory generated in this fashion should provide an excellent guess to initiate a local search for a solution to the semiclassical boundary conditions. Since local searches are tractable even in many dimensions (where a global search would be out of the question) this insight promises to make the semiclassical coherent state propagator practical for very large systems. The results for some preliminary test cases were very promising<sup>21</sup> and in this article we further explore the accuracy and feasibility of this approach by examining the semiclassical coherent state dynamics for some  $N$ -dimensional Henon–Heiles model potentials. We compare the spectra obtained with the present method to

<sup>a)</sup>Author to whom correspondence should be addressed; present address: Dept. of Chemistry, Rm 6-229, Massachusetts Institute of Technology, Cambridge, MA 02139; electronic mail: tvan@mit.edu

those of the Herman–Kluk approach and find that the new method appears to be quite competitive both in terms of accuracy and computational cost.

## II. THE SEMICLASSICAL PROPAGATOR

### A. The classical action

We briefly sketch the derivation of the semiclassical coherent state propagator both to make our notation clear and lay the groundwork for future discussion. We will primarily follow the derivation of Baranger<sup>15</sup> but similar derivations are also available.<sup>12,13</sup> We are interested in a semiclassical approximation to matrix elements of the form (in units where  $\hbar = 1$ )

$$\langle \mathbf{q}_f, \mathbf{p}_f | e^{-i\hat{H}t} | \mathbf{q}_i, \mathbf{p}_i \rangle, \quad (1)$$

where  $\langle \mathbf{q}_f, \mathbf{p}_f |$  and  $| \mathbf{q}_i, \mathbf{p}_i \rangle$  are arbitrary harmonic oscillator coherent states, which can be expanded in terms of position eigenstates as

$$\langle \mathbf{x} | \mathbf{q}, \mathbf{p} \rangle = \left( \frac{\det \gamma}{\pi} \right)^{1/4} \exp - \frac{1}{2} (\mathbf{x} - \mathbf{q})^T \cdot \gamma \cdot (\mathbf{x} - \mathbf{q}) - i \mathbf{p} \cdot \left( \mathbf{x} - \frac{\mathbf{q}}{2} \right). \quad (2)$$

The parameters  $\mathbf{q}$  and  $\mathbf{p}$  fix the average position  $\langle \hat{\mathbf{x}} \rangle$  and momentum  $\langle \hat{\mathbf{p}} \rangle$  for the coherent state and the matrix  $\gamma$  controls the width of the state in position space. Within the semiclassical framework, the value of  $\gamma$  is completely arbitrary since changing it amounts to a canonical transformation of  $\mathbf{p}$  and  $\mathbf{q}$ . Hence without loss of generality, we will replace  $\gamma$  with the identity matrix in what follows. Also, the classical equations are often simplified by working in terms of the complex parameters  $\mathbf{z} = (\mathbf{q} + i\mathbf{p})/\sqrt{2}$  instead of the real parameters  $\mathbf{q}$  and  $\mathbf{p}$ . We will use both notations in what follows, but the meaning should be clear from the context.

In order to obtain a semiclassical approximation to Eq. (1) we follow the canonical prescription of time slicing the quantum propagator and then making stationary phase approximations to the resulting path integral. The first step in time slicing Eq. (1) is to make an appropriate expansion of the identity operator. One possibility is<sup>1</sup>

$$\hat{I} = \int | \mathbf{z} \rangle \langle \mathbf{z} | d\mathbf{z} \wedge d\mathbf{z}^*, \quad (3)$$

where  $\mathbf{z}^*$  is the complex conjugate of  $\mathbf{z}$ . However, for reasons that will become clear later, it is advantageous to consider the following alternative:

$$\hat{I} = e^{+\mathbf{u}^* \hat{\mathbf{a}}} \hat{I} e^{-\mathbf{u}^* \hat{\mathbf{a}}} = \int e^{+\mathbf{u}^* \hat{\mathbf{a}}} | \mathbf{z} \rangle \langle \mathbf{z} | e^{-\mathbf{u}^* \hat{\mathbf{a}}} d\mathbf{z} \wedge d\mathbf{z}^*, \quad (4)$$

where  $\hat{\mathbf{a}} = (\hat{\mathbf{q}} + i\hat{\mathbf{p}})/\sqrt{2}$  is the lowering operator and  $\mathbf{u}$  is an arbitrary complex parameter.

By inserting Eq. (4) into the propagator [Eq. (1)]  $N-1$  times, and rearranging terms, one finds ( $\mathbf{z}_f \equiv \mathbf{z}_N, \mathbf{z}_i \equiv \mathbf{z}_0$ )

$$\int \prod_{j=1}^{N-1} d\mathbf{z}_j \wedge d\mathbf{z}_j^* \prod_{j=1}^N \langle \mathbf{z}_j | e^{-\mathbf{u}_j^* \hat{\mathbf{a}}} e^{-i\hat{H}\epsilon} e^{+\mathbf{u}_{j-1}^* \hat{\mathbf{a}}} | \mathbf{z}_{j-1} \rangle, \quad (5)$$

where  $\epsilon = t/N$  and  $\mathbf{u}_0 \equiv \mathbf{u}_N \equiv 0$ . If we define

$$\hat{H}(\mathbf{u}) \equiv e^{-\mathbf{u}^* \hat{\mathbf{a}}} \hat{H} e^{+\mathbf{u}^* \hat{\mathbf{a}}} \quad (6)$$

then Eq. (5) becomes

$$\int \prod_{j=1}^{N-1} d\mathbf{z}_j \wedge d\mathbf{z}_j^* \prod_{j=1}^N \langle \mathbf{z}_j | e^{-i\epsilon \hat{H}(\mathbf{u}_j)} e^{-(\mathbf{u}_j^* - \mathbf{u}_{j-1}^*) \hat{\mathbf{a}}} | \mathbf{z}_{j-1} \rangle. \quad (7)$$

Finally, if one assumes that  $N$  is large, then  $\epsilon$  and differences such as  $\mathbf{u}_j^* - \mathbf{u}_{j-1}^*$  become small and Eq. (1) reduces to

$$\lim_{N \rightarrow \infty} \int \prod_{j=1}^{N-1} d\mathbf{z}_j \wedge d\mathbf{z}_j^* \prod_{j=1}^N e^{i\epsilon (i\dot{\mathbf{z}}_j \mathbf{z}_j^*/2 - i\dot{\mathbf{z}}_j^* \mathbf{z}_j/2 - i\dot{\mathbf{u}}_j^* \mathbf{z}_j - H(\mathbf{u}_j, \mathbf{z}_j))}, \quad (8)$$

where we have made the natural definitions  $H(\mathbf{u}, \mathbf{z}) \equiv \langle \mathbf{z} | \hat{H}(\mathbf{u}) | \mathbf{z} \rangle$ ,  $\dot{\mathbf{u}}_j^* \equiv (\mathbf{u}_j^* - \mathbf{u}_{j-1}^*)/\epsilon$  and similarly for  $\dot{\mathbf{z}}_j$  and  $\dot{\mathbf{z}}_j^*$ . Hence, we see that the unusual form of the identity [Eq. (4)] modifies the dynamics so that they are governed by an effective Hamiltonian,  $\hat{H}(\mathbf{u}_j)$ , that is a similarity transformation (ST) of the original Hamiltonian. A ST cannot change the spectrum of an operator but can change the eigenfunctions, most notably by making the right eigenfunctions different from the left ones. In our case, the similarity transformation gives us the freedom to adapt the Hamiltonian so that its left and right eigenfunctions are optimally suited to the particular bra and ket coherent states we have chosen. The quantum expression is, of course, unchanged by our choice of  $\mathbf{u}_j$ , since Eq. (8) is exact. However, once we start making approximations, the adaptive freedom afforded by the choice of  $\mathbf{u}$  will be crucial.

Alternatively, one can write Eq. (8) in terms of  $\bar{\mathbf{z}} \equiv \mathbf{z}^* + \mathbf{u}^*$  and  $\mathbf{z}$

$$\lim_{N \rightarrow \infty} \int \prod_{j=1}^{N-1} d\mathbf{z}_j \wedge d\mathbf{z}_j^* \prod_{j=1}^N e^{i\epsilon (i\dot{\bar{\mathbf{z}}}_j \mathbf{z}_j/2 - i\dot{\mathbf{z}}_j \bar{\mathbf{z}}_j/2 - H(\bar{\mathbf{z}}_j, \mathbf{z}_j))}, \quad (9)$$

where  $H(\bar{\mathbf{z}}, \mathbf{z}) \equiv \langle \bar{\mathbf{z}}^* | \hat{H} | \mathbf{z} \rangle$  and it should be clear that  $\bar{\mathbf{z}}$  is not the complex conjugate of  $\mathbf{z}$  (unless, of course,  $\mathbf{u} = 0$ ). This expression for the propagator masks the effect of the similarity transformation, but is algebraically simpler and ultimately has a closer connection with existing work.<sup>13,15</sup> Further, the variables  $\mathbf{z}$  and  $\bar{\mathbf{z}}$  have the concrete value of being associated with the ket and bra states, respectively, which is often useful for physical interpretations.

We are now ready to make the semiclassical limit. To do this, one must perform each of the  $N-1$  integrations over  $d\mathbf{z}_j \wedge d\mathbf{z}_j^*$  by stationary phase. Then, to obtain a final expression, one exploits the  $N \rightarrow \infty$  limit to turn the discrete time expression into a continuous time equivalent that depends on the stationary path  $\{\mathbf{z}(t), \bar{\mathbf{z}}(t)\}$ . This is quite tedious and in this respect our derivation does not differ significantly from previous treatments<sup>12,13,15</sup> and so we merely adapt their results to conform to the present notation. After performing the appropriate manipulations, one finds

$$\langle \mathbf{z}_f | e^{-i\hat{H}t} | \mathbf{z}_i \rangle \approx \sqrt{\frac{i\delta^2 S_{cl}}{\delta \mathbf{z}_i \delta \mathbf{z}_f}} e^{i(S_{cl} - \phi_e)}, \quad (10)$$

where the classical action is given by

$$S_{cl} \equiv \int_0^t \frac{i(\dot{\bar{z}}\bar{z} - \dot{z}z)}{2} - H(\bar{z}, z) d\tau - \frac{i((z(t) - \bar{z}^*(t))\bar{z}(t) + (\bar{z}(0) - z^*(0))z(0))}{2}. \quad (11)$$

The second term in the action is a boundary term that arises because  $z^*$  and  $\bar{z}$  are not the same at the endpoints; that is, it arises because  $u$  is not zero.<sup>11-13,15</sup> The boundary terms fix the otherwise unconstrained variations in the initial and final values of  $u$ . There is also an “extra phase,”  $\phi_e$ , appearing in the exponential in Eq. (10)

$$\phi_e \equiv \frac{1}{2} \text{Tr} \int_0^t \frac{\partial^2 H}{\partial z \partial \bar{z}} d\tau. \quad (12)$$

The form of  $\phi_e$  was first deduced by Solari.<sup>13</sup> However, it was subsequently noticed by Kurchan *et al.*<sup>22</sup> that to leading order in  $\hbar$

$$S_{cl} - \phi_e \approx \tilde{S}_{cl} \equiv \int_0^t \frac{i(\dot{\bar{z}}\bar{z} - \dot{z}z)}{2} - H_W(\bar{z}, z) d\tau - \frac{i((z(t) - \bar{z}^*(t))\bar{z}(t) + (\bar{z}(0) - z^*(0))z(0))}{2}, \quad (13)$$

where  $H_W$  is the Weyl, or symmetrized, symbol for  $H$ . For Hamiltonians of the form  $\hat{H} = T(\hat{p}) + V(\hat{q})$ ,  $H_W(\bar{z}, z)$  can be obtained by making the replacements

$$\hat{q} \Rightarrow \frac{z + \bar{z}}{\sqrt{2}}, \quad \hat{p} \Rightarrow \frac{z - \bar{z}}{i\sqrt{2}}. \quad (14)$$

In practice, we have found that running dynamics using the Weyl Hamiltonian is much more accurate than using the averaged Hamiltonian  $H(\bar{z}, z)$  plus the “extra phase”  $\phi_e$ . Since the two choices are equivalent to leading order in  $\hbar$ , we choose the former and write

$$\langle z_f | e^{-i\hat{H}t} | z_i \rangle \approx \sqrt{\frac{i\delta^2 \tilde{S}_{cl}}{\partial z_i \partial z_f}} e^{i\tilde{S}_{cl}}. \quad (15)$$

To summarize, then, the action we use differs from what one might naively expect in two respects: first, the system evolves under a similarity transformed version of the original Hamiltonian, and second, the classical analog of the quantum Hamiltonian is given by the Weyl symbol rather than the average value of  $\hat{H}$ . It is an open question as to why the Weyl representation is so much better, but we have found this to be the case quite generally.

### B. The equations of motion

Equation (15) is only correct if it is evaluated along the appropriate stationary path  $\{z(t), \bar{z}(t)\}$ . The equations of motion for this path are obtained by making the action,  $\tilde{S}_{cl}$ , stationary with respect to variations in  $z$  and  $\bar{z}$

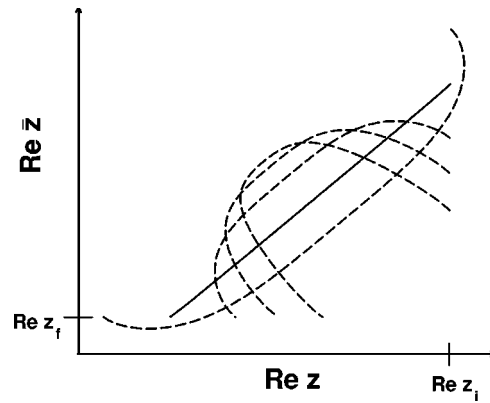


FIG. 1. Several classical trajectories connecting  $z_i$  to  $z_f$  for various time intervals. The solid line is the isolated solution for which  $\bar{z} = z$ .

$$\dot{z} = -i \frac{\partial H_W(\bar{z}, z)}{\partial \bar{z}}, \quad \dot{\bar{z}} = i \frac{\partial H_W(\bar{z}, z)}{\partial z}. \quad (16)$$

One sees immediately that these equations are bivariational; the equations of motion for the variables associated with the left state ( $\bar{z}$ ) are different from those associated with the right state ( $z$ ). This is a natural consequence of the fact that the similarity transformed Hamiltonian is not Hermitian, and thus left and right states are treated differently. The boundary conditions of the classical path are fixed by the initial and final coherent states

$$\bar{z}(t) = z_f^* \quad z(0) = z_i. \quad (17)$$

If  $z$  was our only undetermined variable, we could not expect to solve Eqs. (17) because there would be twice as many constraints as free variables. However, by using the similarity transformation, we introduce a new variable ( $u$ , or equivalently  $\bar{z}$ ) that can be adjusted so that the boundary conditions are satisfied exactly. Hence, it is the boundary values that force the asymmetry of the left and right dynamics.

The structure of the classical path  $\{z(t), \bar{z}(t)\}$  is perhaps best illustrated pictorially. Unfortunately, even for one dimensional problems, this proves difficult since the classical dynamics occurs in a two-dimensional complex space, which would require four real dimensions for a complete representation. However, one can obtain a qualitative picture of what is going on by looking at, say, just the real parts of  $z$  and  $\bar{z}$  as a function of time. This is done for a particular case in Fig. 1. Here, the lines depict different classical solutions to the boundary conditions [Eqs. (17)] for different elapsed times  $t$ . The straight line comes from the isolated solution  $z = \bar{z}$  (i.e.,  $u = 0$ ); clearly the similarity transformation is necessary at all other times if one wishes to find a solution of Eqs. (17). Further, it is also clear that the similarity transform modifies the dynamics in a strongly nonlinear way and so any linearization is only likely to be accurate in special cases. Another way of visualizing the trajectories is to plot  $z$  and  $\bar{z}$  simultaneously on the same complex plane.<sup>12,23,24</sup> This has the advantage of being a more complete description, but can also be misleading since the results then look like two different trajectories, when they should properly be considered two components of the same trajectory.

Finally, we note that the prefactor in Eq. (15) is simply related to the stability matrix elements<sup>15,17–19</sup>

$$i \frac{\delta^2 \bar{S}_{cl}}{\delta \mathbf{z}_i \delta \mathbf{z}_f} = \frac{\delta \bar{\mathbf{z}}(t)^{-1}}{\delta \bar{\mathbf{z}}(0)}. \quad (18)$$

The stability matrix can be computed by integrating the matrix equation

$$\begin{pmatrix} \frac{\delta \dot{\mathbf{z}}(t)}{\delta \mathbf{z}(0)} & \frac{\delta \dot{\mathbf{z}}(t)}{\delta \bar{\mathbf{z}}(0)} \\ \frac{\delta \ddot{\mathbf{z}}(t)}{\delta \mathbf{z}(0)} & \frac{\delta \ddot{\mathbf{z}}(t)}{\delta \bar{\mathbf{z}}(0)} \end{pmatrix} = \begin{pmatrix} \frac{\partial \dot{\mathbf{z}}(t)}{\partial \mathbf{z}(t)} & \frac{\partial \dot{\mathbf{z}}(t)}{\partial \bar{\mathbf{z}}(t)} \\ \frac{\partial \ddot{\mathbf{z}}(t)}{\partial \mathbf{z}(t)} & \frac{\partial \ddot{\mathbf{z}}(t)}{\partial \bar{\mathbf{z}}(t)} \end{pmatrix} \times \begin{pmatrix} \frac{\delta \mathbf{z}(t)}{\delta \mathbf{z}(0)} & \frac{\delta \mathbf{z}(t)}{\delta \bar{\mathbf{z}}(0)} \\ \frac{\delta \bar{\mathbf{z}}(t)}{\delta \mathbf{z}(0)} & \frac{\delta \bar{\mathbf{z}}(t)}{\delta \bar{\mathbf{z}}(0)} \end{pmatrix} \quad (19)$$

along the classical path. The solution of this matrix of differential equations turns out to be the most expensive step in the calculation, scaling with the third power of system size.

### C. Finding the classical paths

Historically, the most challenging part of evaluating the semiclassical propagator of Eq. (15) has been finding the classical paths that satisfy the boundary conditions [Eqs. (17)]. Solutions have only been found where symmetry dictates a particularly simple form for the classical paths<sup>25,26</sup> or in one dimensional systems where a brute force search of the entire complex phase space can be carried out and then the correct solutions can be identified by visual inspection.<sup>16,17,19,23,24,27–29</sup> Thus, applications of Eq. (15) have been limited.

In classical mechanics, one ideally likes to solve initial value problems rather than boundary value problems, and so it is helpful to view this problem from an initial value perspective.<sup>30,31</sup> If we take the initial values  $\bar{\mathbf{z}}(0)$  and  $\mathbf{z}(0)$  as our independent variables, then  $\bar{\mathbf{z}}(t)$  becomes an implicit function of the independent variables and our boundary conditions become

$$\bar{\mathbf{z}}(t; \bar{\mathbf{z}}(0), \mathbf{z}(0)) = \mathbf{z}_f^* \quad \mathbf{z}(0) = \mathbf{z}_i. \quad (20)$$

The second equality is trivial, but the first relation is, in general, a set of nonlinear equations in  $\bar{\mathbf{z}}(0)$  and  $\mathbf{z}(0)$  that is difficult to solve. However, assuming one has in hand a good initial approximation to the desired starting conditions, the Newton–Raphson (NR) approach provides a reliable solution to our boundary value problem.<sup>32</sup> The key step is the solution of an  $\mathbf{A} \cdot \mathbf{x} = \mathbf{b}$  problem where  $\mathbf{b}$  is the error in the above equations

$$\mathbf{b} \equiv \begin{pmatrix} \bar{\mathbf{z}}(t) - \mathbf{z}_f^* \\ \mathbf{z}(0) - \mathbf{z}_i \end{pmatrix} \quad (21)$$

and  $\mathbf{A}$  is the Jacobian

$$\mathbf{A} \equiv \begin{pmatrix} -\partial \mathbf{b} & -\partial \mathbf{b} \\ \frac{\partial \mathbf{z}(0)}{\partial \bar{\mathbf{z}}(0)} & \frac{\partial \mathbf{z}(0)}{\partial \bar{\mathbf{z}}(0)} \end{pmatrix} = \begin{pmatrix} -\frac{\delta \bar{\mathbf{z}}(t)}{\delta \bar{\mathbf{z}}(0)} & -\frac{\delta \bar{\mathbf{z}}(t)}{\delta \bar{\mathbf{z}}(0)} \\ -1 & 0 \end{pmatrix}. \quad (22)$$

Given any approximate solution to the boundary conditions,  $\mathbf{x}$  is the first-order correction to  $\{\bar{\mathbf{z}}(0), \mathbf{z}(0)\}$ . Hence, the true solution can be approximated by

$$\begin{pmatrix} \bar{\mathbf{z}}_{\text{exact}}(0) \\ \mathbf{z}_{\text{exact}}(0) \end{pmatrix} \approx \begin{pmatrix} \bar{\mathbf{z}}(0) \\ \mathbf{z}(0) \end{pmatrix} + \mathbf{x} \quad (23)$$

and this process is iterated until the steps are smaller than a given cutoff. The convergence is quadratic, and so the process works well as long as one is “near” the solution. Of course, NR becomes inaccurate when the steps are large and so in practice it is useful to scale the correction  $\mathbf{x}$  when it is larger than some fixed value (e.g., 1). Finally, it is worth noting that the NR procedure makes use of the same stability matrix elements that the semiclassical propagator [Eq. (15)] requires. Thus, the only additional effort in the NR search arises from the fact that multiple trajectories will need to be run before convergence is achieved.

Now, as mentioned above, NR is only useful when one has a good approximation to the desired initial conditions. We have recently shown<sup>21</sup> that a good guess is provided by initial conditions that almost connect  $\mathbf{z}_i$  to  $\mathbf{z}_f$  when run with the untransformed Hamiltonian, i.e., trajectories for which  $\bar{\mathbf{z}} = \mathbf{z}$ . This can be justified in several ways. On the one hand, it has long been known that more rudimentary semiclassical techniques that utilize the untransformed Hamiltonian often provide a realistic description of quantum dynamics.<sup>2–4,33</sup> Therefore, we already know empirically that the untransformed dynamics will provide a physically reasonable starting point for the more sophisticated transformed semiclassical propagator; in this respect, our approach is not unlike the “off-center guiding” approximation useful for highly chaotic systems.<sup>34</sup> Alternatively, it can be shown for simple systems that, to leading order, a solution with smaller  $\mathbf{u}$  will be exponentially dominant over one that requires a larger  $\mathbf{u}$ <sup>15,17</sup> and thus solutions that are “near” the untransformed dynamics (where  $\mathbf{u} = 0$ ) should be the most important. Hence, one should not be entirely surprised if this approach is effective—it is only a question of *how* effective it can be.

On the other hand, one might have concerns about the feasibility of this suggestion; how close does an untransformed trajectory need to be to the transformed solution in order for the NR iterations to converge? Mathematically, the trajectory needs to be within the radius of convergence of the NR procedure, and for unstable periodic orbits it has been shown<sup>35</sup> that the NR procedure can converge to a given orbit even when the initial guess is 100 times further away than the basin of stability would imply! This is quite astonishing and points strongly toward the possibility that one should be able to find untransformed solutions that are “close enough” (in the NR sense) without a large expenditure of work, even for chaotic systems. Indeed, we find in practice that our boundary value problem is inherently better conditioned than the periodic orbit problem (perhaps due to the presence of zero frequency modes in the latter)<sup>35</sup> and further that solutions that have small islands of convergence tend to make small contributions to the semiclassical propagator. It is not yet clear whether this last observation can be justified mathematically (e.g., by finding an approximate relation be-

tween the area of the island and the magnitude of the contribution) but it clearly supports the feasibility of this approach.

Of course, the untransformed trajectories will only come near the desired endpoint for particular, characteristic, times (e.g., classical recurrences of the system) and so it becomes necessary to trace out branches of solutions that are continuously connected to an isolated solution. This is done by NR; given a solution at a particular time, a solution at a nearby time can be obtained using the initial conditions of the nearby time as a guess. By making small steps forward and backward in time and repeating the NR procedure at each step a particular solution naturally leads to an entire branch of solutions. These other contributions must be included if we want the propagator to be continuous in time. Further, since all of the solutions on a given branch can be continuously deformed into the original solution, one is often able to glean insight into the problem from the structure of a branch (e.g., one can assign it to a particular physical motion of the system).

To summarize, then, our algorithm for computing the semiclassical coherent state propagator [Eq. (15)] is as follows.

- (1) Choose several initial conditions close to  $\mathbf{z}_i$  and propagate them forward in time using the untransformed classical Hamiltonian  $H_W(\mathbf{z})$ . In many cases,  $\mathbf{z}_i$  yields all the important recurrences by itself, but in cases with symmetry constraints or with strong temporal overlap between different branches, it becomes necessary to run a few (e.g., 10–20) initial conditions to ensure that all important branches are captured.
- (2) For each time one of the above trajectories comes “near” the final point, perform a NR search to find the nearest solution to the boundary conditions [Eq. (17)].
- (3) For each solution found in the last step, take small steps forward and backward in time to trace out a branch of solutions. For each new time, the solution at the previous time is used as a guess for the NR procedure.
- (4) Compute the semiclassical propagator [Eq. (15)] along each branch.
- (5) Add all the contributions computed in the last step to obtain the full propagator.

Care must be taken here when computing the relative phases of different branches, due to the indeterminate sign of the square root in Eq. (15). Within a given branch, the relative phases can be assigned by requiring that the signal be a continuous function of time. The overall phase for a given branch is more difficult to determine because of the presence of caustics between the initial and final points. However, for trajectories near the untransformed solution caustics are very uncommon and so the overall phase can be easily computed using one of these trajectories and choosing the sign of the square root consistently as the trajectory is propagated.<sup>7,36</sup>

Finally, we note that our approach is a generalization of Klauder’s proposition<sup>20</sup> that “continuously connected” paths are the most important for the semiclassical propagator. The work of Grossmann on semiclassical scattering advocates this hypothesis.<sup>18</sup> In the language of this paper, the “continuously connected” paths are the branch of solutions that

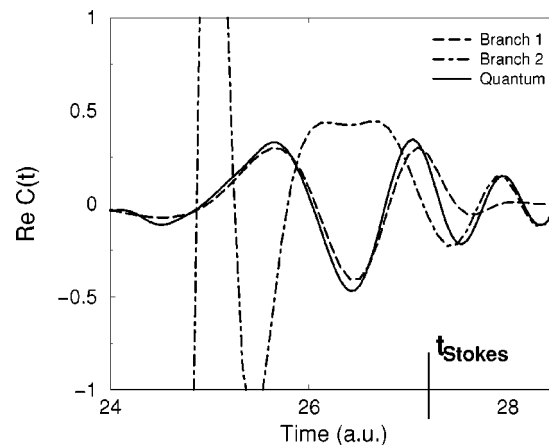


FIG. 2. Two different branches that contribute to the two-dimensional Henon–Heiles propagator. The first branch is dominant to the left of the Stokes line while the second is dominant to the right. The exponential blowup of the second branch is erroneous.

connect to the zero time result. By including not only this branch, but branches that arise from later recurrences of the untransformed Hamiltonian, our results will be superior for later times when multiple branches are present and interference between these branches is significant.<sup>21</sup>

### III. STOKES’ PHENOMENON AND CAUSTICS

Stokes’ phenomenon generically arises when one approximates an integral or differential equation by the sum of two or more contributions;<sup>37,38</sup> in our case, we are approximating the quantum path integral by a sum of different semiclassical branches, and so it should come as no surprise that we must deal with Stokes’ phenomenon. Assuming for simplicity that there are only two branches, within the semiclassical approximation we can write

$$\langle \mathbf{z}_f | e^{-i\hat{H}t} | \mathbf{z}_i \rangle \approx M_1(t) e^{i\tilde{S}_1(t)} + M_2(t) e^{i\tilde{S}_2(t)}, \quad (24)$$

where  $M_1$  and  $M_2$  are the appropriate stability prefactors, as in Eq. (15). A Stokes line occurs when  $\text{Re } \tilde{S}_1(t) = \text{Re } \tilde{S}_2(t)$  and around this line the relative importance of these two terms changes rapidly. Roughly speaking, for  $t < t_{\text{Stokes}}$  one contribution is expected to be more accurate while for  $t > t_{\text{Stokes}}$  the other branch is to be preferred. By convention, we label the two signals so that “1” is preferred at shorter times and “2” is dominant at longer times. Now, often the process of one branch “switching on” while the other “switches off” happens naturally; for example branch “2” may decay exponentially before  $t_{\text{Stokes}}$ . However, it is equally possible for the second contribution to grow exponentially for times  $t < t_{\text{Stokes}}$  resulting in the undesirable result that branch “2” could swamp the signal from branch “1” even at times where branch “1” is expected to be very accurate!

An illustration is useful at this point. Figure 2 shows two branches that contribute to the Henon–Heiles model problem discussed in Sec. IV. The Stokes line is marked with a vertical hash, and the quantum result is also shown for comparison. Clearly the second branch is accurate for times to the right of  $t_{\text{Stokes}}$  and the first branch is accurate for times to the

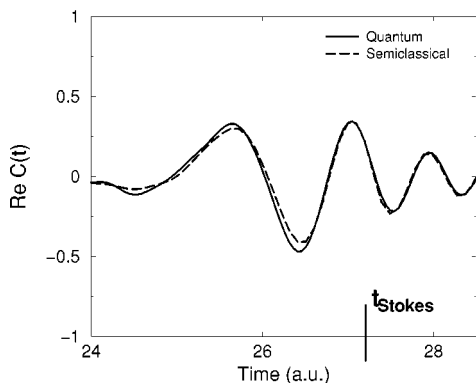


FIG. 3. The semiclassical propagator obtained by combining the two branches from Fig. 2 using Eq. (25).

left; but the second branch blows up exponentially in this region. If we simply add these two contributions, we will get garbage.

Clearly what is required is some universal function, that “switches off” the second branch in cases where this does not naturally occur. Luckily for us, Berry has derived just such a function.<sup>39</sup> He begins by considering the asymptotic expansion of the integral in powers of  $1/\hbar$  and identifying a series of diverging terms. He then proceeds to analytically resum this series and show that the result kills off the divergence of the subdominant branch when it is on the “wrong” side of the Stokes line. In the end, one obtains the modified expression

$$\langle \mathbf{z}_f | e^{-i\hat{H}t} | \mathbf{z}_i \rangle \approx M_1(t) e^{i\tilde{S}_1(t)} + G(t) M_2(t) e^{i\tilde{S}_2(t)}, \quad (25)$$

where the Stokes multiplier,  $G(t)$  is given by

$$G(t) = \frac{1}{2} \left( 1 - \operatorname{erf} \left[ \frac{\operatorname{Re}[\tilde{S}_1(t) - \tilde{S}_2(t)]}{\sqrt{2 \operatorname{Im}[\tilde{S}_2(t) - \tilde{S}_1(t)]}} \right] \right). \quad (26)$$

Berry’s result is extremely general, applying to asymptotic expansions in the large, and so one feels very comfortable appropriating this for use in a wide variety of physical circumstances. Also, it is worth noting that the Stokes multiplier becomes undefined when one passes an anti-Stokes line, where  $\operatorname{Im} \tilde{S}_1(t) = \operatorname{Im} \tilde{S}_2(t)$ . These lines typically appear on either side of the Stokes line, and so the smoothing only affects a relatively narrow region about the Stokes line. Outside this region,  $G(t)$  is taken to be 1 or 0 as appropriate.

The amazing thing about Berry’s Stokes multiplier is that it doesn’t require any information except for the branches and the classical actions associated with them. By adding overlapping branches using Eq. (26) rather than Eq. (24) one can remove inaccurate contributions that appear on the “wrong” side of a Stokes line. For example, if we use Eq. (25) to add up the two contributions in Fig. 2—one of which is clearly divergent—we obtain the result in Fig. 3, which is not only smooth, but also quite faithful to the quantum result.

The other problem that tends to plague semiclassical approaches is the appearance of caustics. We have not found caustics to be very prevalent in the correlation functions we have examined and this can be understood in one of two

ways. First, while previous studies have uncovered caustic singularities in the semiclassical coherent state propagator,<sup>16,17,20</sup> it has been noted<sup>16,28</sup> that these caustics also create Stokes’ lines. As one might expect, we have found that these caustics usually lie on the “wrong” side of a Stokes line, and therefore make no contribution to the semiclassical propagator once Stokes’ multiplier [Eq. (26)] is taken into account. Another way to understand the absence of singularities in our results is to recall that the untransformed classical dynamics of coherent states have no caustic singularities.<sup>40</sup> Thus, as long as one remains inside a thin shell “near” these trajectories, caustics should, by continuity, nearly always be absent. Hence, by selecting branches that are “near” the untransformed dynamics, we not only select the dominant contributions, but also those most likely to be free of caustic singularities. Of course, caustics will show up in some cases, but by toying with the choice of boundary conditions one should be able to select correlation functions where the effect of caustics is acceptably small.

#### IV. APPLICATION TO HENON–HEILES MODEL POTENTIALS

As an application of the similarity transformed dynamics, we consider the  $N$ -dimensional Henon–Heiles model Hamiltonian<sup>41</sup>

$$H(\hat{\mathbf{p}}, \hat{\mathbf{q}}) = \frac{1}{2} \hat{\mathbf{p}}^2 + V(\hat{\mathbf{q}}), \quad (27)$$

where the potential is given by

$$V(\hat{\mathbf{q}}) \equiv \frac{1}{2} \hat{\mathbf{q}}^2 + 0.11803 \sum_{j=1}^{N-1} (q_j^2 q_{j+1} - q_j^3/3). \quad (28)$$

This is a simple generalization of the two dimensional Henon–Heiles potential of Heller<sup>33</sup> to higher dimensions. It retains the anharmonic coupling of the original model and the metastability of every mode with respect to dissociation. We are interested in the Franck–Condon absorption spectrum<sup>42</sup> of this system

$$I(E) = \frac{1}{2\pi} \int_{-\infty}^{\infty} e^{iEt} \langle \mathbf{z} | e^{-i\hat{H}t} | \mathbf{z} \rangle dt, \quad (29)$$

where  $z_j = 2$  for  $j = 1, 2, \dots, N$ . If this were a bound system, then the spectrum would consist of a series of sharp lines at each of the eigenvalues of  $H(\hat{\mathbf{p}}, \hat{\mathbf{q}})$  and the intensities would represent the weight of the relevant eigenstate in  $|\mathbf{z}\rangle$ . However, since we are dealing with a quasibound system, one no longer has eigenstates, but only resonances. Every resonance has a finite lifetime, which gives each line in the spectrum a finite width. Hence, we will be interested in extracting the positions, heights, and widths of the peaks using our semiclassical approach. This is done in a straightforward manner by approximating the matrix element  $\langle \mathbf{z} | e^{-i\hat{H}t} | \mathbf{z} \rangle$  using Eq. (15) and then taking the Fourier transform to obtain the spectrum.

These Franck–Condon spectra were also computed semiclassically in Ref. 41 using the popular method of Herman and Kluk (HK).<sup>6</sup> In the present notation, the HK approximation takes the form

$$\langle \mathbf{z} | e^{-i\hat{H}t} | \mathbf{z} \rangle \approx \int \langle \mathbf{z} | \mathbf{w}(t) \rangle \sqrt{\left| \frac{\delta \mathbf{w}(t)}{\delta \mathbf{w}(0)} \right|} e^{i\tilde{S}_{cl}(\mathbf{w},t)} \langle \mathbf{w}(0) | \mathbf{z} \rangle \times d\mathbf{w}(0) \wedge d\mathbf{w}^*(0). \quad (30)$$

Here,  $\mathbf{w}(t)$  is the classical trajectory that evolves from  $\mathbf{w}(0)$  under the untransformed Hamiltonian, so that  $\bar{\mathbf{w}} = \mathbf{w}^*$  at all times. The action [Eq. (13)] is the same as before, but the boundary terms vanish because  $\bar{\mathbf{w}} = \mathbf{w}^*$ . The equations of motion [Eq. (16)] are unaltered but the trajectory now only needs to satisfy the trivial boundary conditions

$$\bar{\mathbf{w}}(t) = \mathbf{w}^*(t) \equiv \mathbf{w}_f^* \quad \mathbf{w}(0) \equiv \mathbf{w}_i. \quad (31)$$

Clearly the two propagators [Eqs. (15) and (30)] involve very similar operations; the major difference is that the HK propagator circumvents the boundary value search by integrating over the initial phase space. This is motivated by the observation that every initial value leads to *some* final value and thus if one includes all initial values, one accounts for all possible final values as well. It is for this reason that HK and expressions like it are often termed “initial value representations.”<sup>7,31,36</sup>

At the same time, the integrand in Eq. (30) is weighted by the two overlap factors  $\langle \mathbf{w}(0) | \mathbf{z} \rangle$  and  $\langle \mathbf{z} | \mathbf{w}(t) \rangle$  and hence it will only be large if both the initial and final values of the untransformed trajectory are *near*  $\mathbf{z}$ . For a typical system, most trajectories will not begin or end anywhere near  $\mathbf{z}$  and thus the integrand will be zero for all but a very small region of phase space. Hence, there is a need for an efficient method of biasing the integration so that only the significant values of  $\mathbf{w}(0)$  are propagated. The simplest method for doing this is to use the initial overlap,  $|\langle \mathbf{w}(0) | \mathbf{z} \rangle|$ , as a weight function from which initial values are sampled in a Monte Carlo integration. But this ignores the equally important final overlap factor, and one therefore ends up running a large number of trajectories that begin near the initial point but end up nowhere near the desired final point. There have been various sampling techniques proposed to solve this problem: One can do importance sampling based on the behavior of the trajectory at intermediate times,<sup>43</sup> reduce the number of trajectories by time averaging,<sup>44</sup> or one can smooth the integrand by applying various Gaussian filters to it.<sup>45,46</sup> In this respect, the Henon–Heiles problem is a rather stringent test case, since the number of trajectories needed to accurately compute the propagator can vary by a factor of 100, depending on what type of smoothing function one employs.<sup>41,46</sup>

Instead of beginning from a random search and attempting to throw out terms that are unimportant, our approach can be viewed as beginning from the terms that are sure to be significant—those that begin and end near the boundary points—and using those to extract as much information as possible about the propagator. This approach is guaranteed to be computationally efficient, since no insignificant contributions will be generated, and the only question, then, is whether it is accurate. Thus, in what follows we shall investigate the agreement between the HK results and our similarity transformed dynamics in the hopes of determining the reliability of our scheme for selecting the most significant branches.

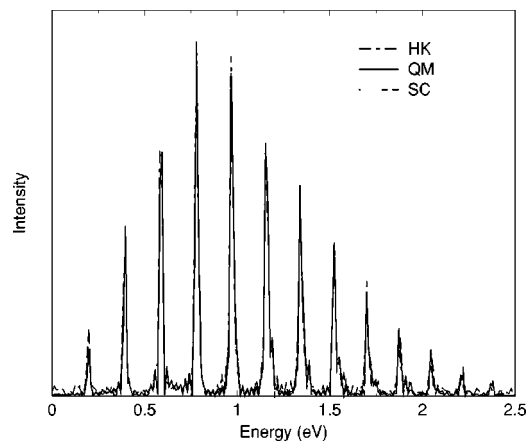


FIG. 4. Franck–Condon spectra for the two-dimensional Henon–Heiles system using the present semiclassical propagator (SC), Herman–Kluk (HK), and quantum dynamics (QM).

### A. Franck–Condon spectra

We first present our results for the two dimensional Henon–Heiles problem, because this system affords the additional luxury of a comparison to exact quantum dynamics obtained using the split-operator technique of Feit and Fleck.<sup>47</sup> All the spectra were convoluted with a Gaussian window function, as in Ref. 41. The results are quite encouraging; as shown in Fig. 4, the spectra obtained from the present semiclassical propagator, the HK dynamics, and the full quantum simulation all agree essentially quantitatively as to the positions, widths, and intensities of the various resonances. A detailed comparison shows that HK is slightly better than the similarity transformed dynamics at predicting the intensities and widths of the resonances but that the two methods give identical predictions of the center of each peak (within the statistical error of the HK approach). However, both methods are clearly faithful to the exact result and because the same physics is likely to be at work as the dimensionality of the problem increases, one can be fairly confident that both semiclassical methods will give reliable results for the larger models.

For the  $N$ -dimensional potentials with  $N=4, 6, 8$ , and 10 it has recently been shown<sup>48</sup> that the HK spectra agree almost quantitatively with numerically exact multiconfigurational time-dependent Hartree simulations. Thus, for these systems we are justified in using the HK as a benchmark against which our results can be measured. This comparison is presented in Fig. 5. Clearly the agreement between the present method and the established HK results persists as the number of degrees of freedom is increased. Further, the agreement actually appears to improve in the larger models. If we assume the HK results are more reliable, the ST dynamics slightly underestimate the resonance widths for the lower dimensional cases resulting in, for example, an exaggeration of the fringing on the high energy side of the continuum band for  $N=4$ . However, for the  $N=8$  and  $N=10$  cases the two methods agree essentially quantitatively on the depth of the fringes. This can be understood by analyzing the autocorrelation functions of the two models (not shown), whose Fourier transforms give the spectra. In all cases, the

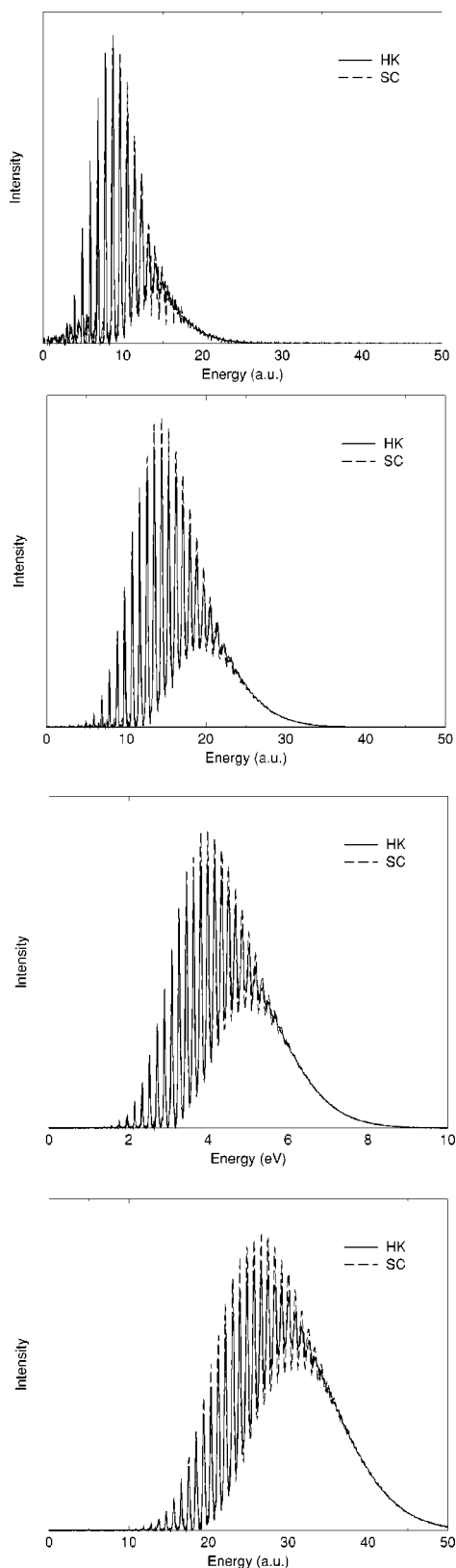


FIG. 5. Franck-Condon spectra for the multidimensional Henon-Heiles system with  $N=4,6,8,10$  degrees of freedom. Results are obtained with the present semiclassical propagator (SC) and Herman-Kluk (HK).

differences between the ST and HK results only show up after several periods of classical oscillation. However, because of the dissipation provided by the additional degrees of

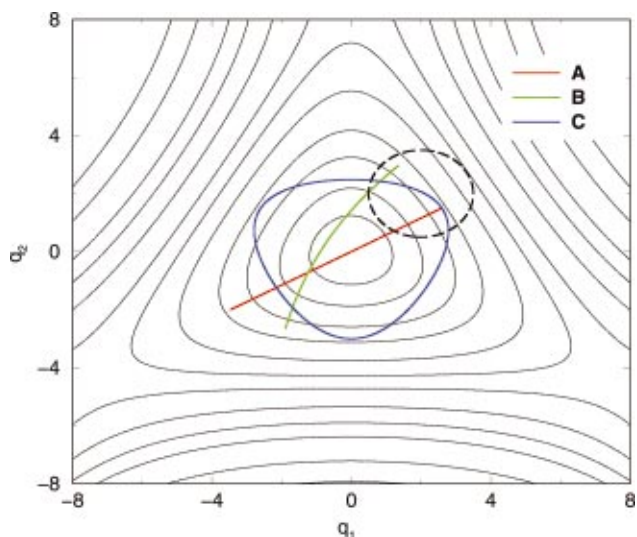


FIG. 6. (Color) The three shortest periodic orbits for the two-dimensional Henon-Heiles model. The dotted lines indicate the contours of the underlying potential. The dashed circle shows the location of the initial wave packet.

freedom, the autocorrelation decays more and more rapidly in time as  $N$  increases. Hence, the differences between the two methods at long times is effectively washed out in the bigger models and we see improved agreement between the spectra.

## B. The stationary paths

As we have noted previously, although the knowledge of the periodic orbits is not required for our search algorithm, the contributions to the autocorrelation function can often be classified by their relationship to the periodic orbits of the untransformed Hamiltonian<sup>21</sup> giving valuable insight into the classical origins of spectral features. The same is true in this case. For example, the three shortest periodic orbits for the two dimensional Henon-Heiles system are shown in Fig. 6. Our search procedure uncovers a series of branches that are associated with the recurrences of the  $A$  orbit that originates from the nearby saddle point. A second series of branches can be associated with successive recurrences of the  $B$  orbit. This allows us to recognize not only the importance of perturbed normal mode motion (which develops into in a  $B$  orbit at the energies we are studying) but also the global potential surface (which gives us the  $A$  orbits) in describing the spectrum. It is also interesting that we find no significant contributions that result from the  $C$  orbit, which correspond to rotations. This is due to our choice of initial wave packet; the total momentum for the  $C$  orbit is never zero, and hence the phase space overlap of this orbit with the  $\mathbf{z}=2$  coherent state is small. We have verified that a different choice of initial conditions for this same model yields important contributions resembling the  $C$  orbit. At longer times and/or higher energies, branches associated with the more complicated orbits that result from period doubling of the basic  $A$  and  $B$  orbits<sup>49</sup> also become significant, but for the present case they provide a negligible contribution.

We wish to stress that these periodic orbits were not used to *find* the branches. The root search was carried out exactly

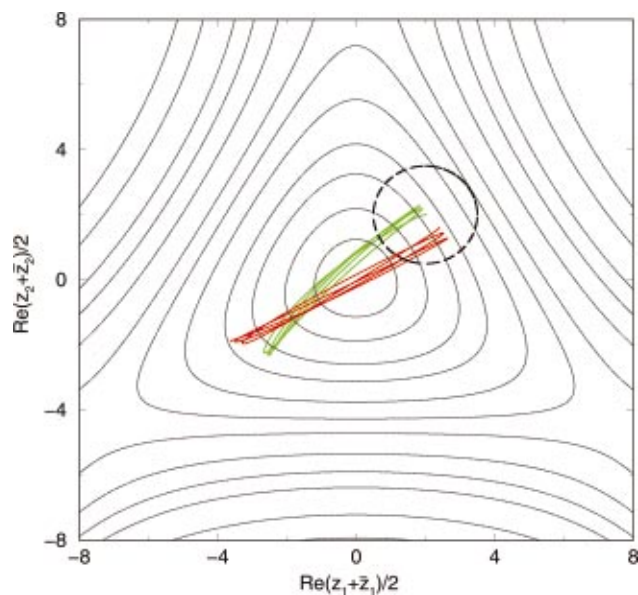


FIG. 7. (Color) Two representative branches for the the two-dimensional Henon–Heiles model. The resemblance to the  $A$  and  $B$  periodic orbits in Fig. 6 is striking.

as described in the previous section; several random initial conditions (in this case, 10–15) near  $\mathbf{z}=2$  were chosen and propagated using the untransformed Hamiltonian. These trajectories were used as initial guesses in the NR search to find nearby branches. Since some of the initial conditions were closer to  $A$  resonances and others were closer to  $B$  resonances, the two classes of branches fall out naturally from this search procedure. For example, two stationary paths that arise directly from our search are depicted in Fig. 7 and it is easy to see that they are related to recurrences of the  $A$  and  $B$  orbits, respectively.

For dimensions greater than three, it is of course not possible to visualize the periodic orbits and we have not performed a search to find the periodic orbits of the higher dimensional Henon–Heiles problems for this reason. However, we can say that for higher dimensions all of the branches we have found arise from recurrences of one periodic orbit; we infer this, for example, from the fact that new branches occur only at regular intervals in time, indicating a single underlying period. We further infer that it is the  $A$ -type branches that are absent from the higher dimensional cases. The  $A$  orbits emanate from the saddle points of the potential and therefore have a maximum energy—the barrier to dissociation—above which motion along the  $A$  axis turns from periodic to dissociative. A simple calculation reveals that for  $N>3$  the initial wave packet energy is actually *above* the lowest saddle point and therefore there are no relevant  $A$ -type orbits in this region of phase space. We thus conclude that the branches we have found for the higher dimensional models all arise from  $B$ -type motions. Of course, as was the case for two dimensions, other initial wave packets will reveal the importance of other classical orbits. For example, if we considered an initial state with lower energy, branches arising from  $A$ -type orbits would presumably reappear.

## V. CONCLUSIONS

In all cases we have studied, untransformed trajectories that almost satisfy the boundary conditions provide the necessary initial conditions in the search for the most significant contributions to the semiclassical coherent state propagator. Further, the present work demonstrates that the number of significant contributions does not increase substantially as the dimension increases, even in the presence of weak chaos. Thus the untransformed dynamics play a crucial role in constructing the full semiclassical propagator in a practical fashion.

Perhaps most importantly, our results show that the semiclassical propagator gives results that are comparable to those of the best available semiclassical techniques (exemplified here by the Herman–Kluk approximation<sup>6</sup>). Yet the present approach requires fewer trajectories than HK even when prescreening techniques are employed in the latter. For example, for the ten-dimensional Henon–Heiles problem,  $\approx 2000$  trajectories are required to solve the boundary value problem for the semiclassical propagator, while 6400 are required to converge the Herman–Kluk integrand.<sup>46</sup> One further benefit of the transformed dynamics is that the results can be obtained to arbitrary precision (if not arbitrary accuracy) with only a modest additional effort. This is to be compared with the Monte Carlo integration implicit in the HK approach, which only converges as  $1/\sqrt{N_{\text{trajectories}}}$ . Hence, we conclude that the semiclassical propagator is a very promising tool for treating the semiclassical dynamics of large systems.

Another appealing aspect of this method relative to some more primitive semiclassical approaches<sup>33</sup> is that the classical Hamiltonian is *not*  $\langle \hat{H} \rangle$ , but instead the Weyl symbol  $H_W$ . For large systems, an accurate global potential energy surface will not generally be available and it is therefore crucial that a method be able to work with data from the present point in phase space that has been generated “on the fly.”  $\langle \hat{H} \rangle$  is nonlocal, since it involves an average over the width of the wave packet. But  $H_W$  is local—it involves replacing the position and momentum by the classical variables  $q$  and  $p$  that define the center of the wave packet. Since  $H_W$  depends on the behavior of  $\hat{H}$  exactly at the center of the wave packet, it is inherently local and easy to obtain “on the fly.” Unfortunately, the similarity transformation introduces the additional complication that the effective values of  $q$  and  $p$  become complex and thus the Hamiltonian function must now be evaluated at a point in *complex* phase space. However, in the common case that one is using an *ab initio* electronic structure method, this can be accomplished by changing the computer programs that generate the potential and its derivatives at a given point  $R$  so that all the variables that were originally constrained to be real are now allowed to be complex. Given the intricacy of *ab initio* packages, this is a challenging task and so one should certainly explore the effectiveness of the present approach further before such a plan is undertaken. However, it is encouraging to know that “on the fly” dynamics are a possibility for transformed semiclassical dynamics.

One open question is how strong chaos will affect the

feasibility of our search algorithm. As the system is made more and more chaotic (e.g., by raising the energy) the number of periodic orbits proliferates more and more rapidly as a function of time. For example, even for fairly simple kicked rotor maps, the semiclassical branch structure becomes impressively convoluted even after 3–5 iterations.<sup>16,27,28</sup> Hence, for highly chaotic problems, one might imagine the existence of hundreds or even thousands of important branches, which would make the root search both tedious and difficult. There are several things that will mitigate this in practice. First, we are typically only interested in moderate times ( $\approx 10$  cycles of the fundamental oscillation) and hence complicated orbits that result from many period doublings of the fundamental orbits are not required. Second, as pointed out in the previous section, we are only interested in orbits that begin near a specified point in phase space—the location of the initial wave packet. Finally, the orbits that are very unstable—and whose branches are typically the most difficult to converge—usually give small contributions to the autocorrelation function. Thus the number of important branches is realistically limited by the number of periodic orbits of short period that pass through a given region of phase space and are not too unstable. Application of the present approach to some strongly chaotic problems should help reveal whether this number ever becomes impractically large, but in the weakly chaotic systems studied here, it is certainly manageable.<sup>50,51</sup>

The observations made here open up a number of promising directions for future applications of the semiclassical propagator. First, one would like to use this technique to describe the semiclassical dynamics of larger, more realistic, systems. For example, one would like to be able to describe the quantum dynamics of realistic cluster models of condensed phase dynamics. In this case, tens or even hundreds of degrees of freedom will come into play and the fact that the present approach scales with just the third power of the system size will be crucial. Alternatively, the high accuracy that is obtained with the present approach leads one to hope that systems that were previously considered “too nonclassical” might now be within the reach of semiclassical analysis. For example, one might use the semiclassical spin coherent state propagator to examine the semiclassical dynamics of electron spins.<sup>52</sup> Extensions to multiple time correlation functions should also be illuminating.

## ACKNOWLEDGMENT

This work was supported by a grant from the National Science Foundation (Grant No. CHE-0073544).

- <sup>1</sup>J. R. Klauder and B. S. Skagerstam, *Coherent States, Applications in Physics and Mathematical Physics* (World Scientific, Singapore, 1985).
- <sup>2</sup>E. J. Heller, *J. Chem. Phys.* **62**, 1544 (1975).
- <sup>3</sup>E. J. Heller, *J. Chem. Phys.* **66**, 5777 (1977).
- <sup>4</sup>E. J. Heller, *J. Chem. Phys.* **67**, 3339 (1977).
- <sup>5</sup>M. J. Davis and E. J. Heller, *J. Chem. Phys.* **71**, 3383 (1979).
- <sup>6</sup>M. F. Herman and E. Kluk, *Chem. Phys.* **91**, 27 (1984).
- <sup>7</sup>K. G. Kay, *J. Chem. Phys.* **100**, 4377 (1994).
- <sup>8</sup>W. H. Miller, *J. Phys. Chem. A* **105**, 2942 (2001).
- <sup>9</sup>N. Makri, *Annu. Rev. Phys. Chem.* **50**, 167 (1999).
- <sup>10</sup>F. Grossmann and A. L. Xavier, Jr., *J. Phys. A* **243**, 243 (1998).
- <sup>11</sup>J. R. Klauder, *Phys. Rev. D* **19**, 2349 (1979).
- <sup>12</sup>Y. Weissman, *J. Chem. Phys.* **76**, 4067 (1982).
- <sup>13</sup>H. G. Solari, *J. Math. Phys.* **27**, 1351 (1986).
- <sup>14</sup>J. R. Klauder, *Random Media* (Springer, New York, 1987), pp. 163–182.
- <sup>15</sup>M. Baranger *et al.*, *J. Phys. A* **34**, 7227 (2001).
- <sup>16</sup>S. Adachi, *Ann. Phys. (N.Y.)* **195**, 45 (1989).
- <sup>17</sup>A. L. Xavier, Jr. and M. A. M. de Aguiar, *Ann. Phys. (N.Y.)* **252**, 458 (1996).
- <sup>18</sup>F. Grossmann, *Phys. Rev. A* **57**, 3256 (1998).
- <sup>19</sup>A. L. Xavier and M. A. M. de Aguiar, *Phys. Rev. Lett.* **79**, 3323 (1997).
- <sup>20</sup>A. Rubin and J. R. Klauder, *Ann. Phys. (N.Y.)* **241**, 212 (1995).
- <sup>21</sup>T. Van Voorhis and E. J. Heller, *Phys. Rev. A* **66**, 050501 (2002).
- <sup>22</sup>J. Kurchan, P. Leboeuf, and M. Saraceno, *Phys. Rev. A* **40**, 6800 (1989).
- <sup>23</sup>D. Huber and E. J. Heller, *J. Chem. Phys.* **87**, 5302 (1987).
- <sup>24</sup>D. Huber, E. J. Heller, and R. G. Littlejohn, *J. Chem. Phys.* **89**, 2003 (1988).
- <sup>25</sup>S. C. Creagh and N. D. Whelan, *Phys. Rev. Lett.* **77**, 4975 (1996).
- <sup>26</sup>S. C. Creagh and N. D. Whelan, *Phys. Rev. Lett.* **82**, 5237 (1999).
- <sup>27</sup>A. Shudo and K. S. Ikeda, *Phys. Rev. Lett.* **74**, 682 (1995).
- <sup>28</sup>A. Shudo and K. S. Ikeda, *Phys. Rev. Lett.* **76**, 4151 (1996).
- <sup>29</sup>A. Shudo and K. S. Ikeda, *Physica D* **115**, 234 (1998).
- <sup>30</sup>W. H. Miller, *Adv. Chem. Phys.* **25**, 69 (1974).
- <sup>31</sup>W. H. Miller, *J. Chem. Phys.* **53**, 3578 (1970).
- <sup>32</sup>The NR method is discussed, for example, in the *Numerical Recipes* books, available at ([www.nr.com](http://www.nr.com)).
- <sup>33</sup>E. J. Heller, *J. Chem. Phys.* **75**, 2923 (1981).
- <sup>34</sup>S. Tomsovic and E. J. Heller, *Phys. Rev. Lett.* **67**, 664 (1991).
- <sup>35</sup>R. Marcinek and E. Pollak, *J. Chem. Phys.* **100**, 5894 (1994).
- <sup>36</sup>K. G. Kay, *J. Chem. Phys.* **100**, 4432 (1994).
- <sup>37</sup>G. Stokes, *Trans. Cambridge Philos. Soc.* **10**, 106 (1864).
- <sup>38</sup>G. Stokes, *Trans. Cambridge Philos. Soc.* **11**, 412 (1871).
- <sup>39</sup>M. V. Berry, *Proc. R. Soc. London, Ser. A* **422**, 7 (1989).
- <sup>40</sup>A. Voros, *Phys. Rev. A* **40**, 6814 (1989).
- <sup>41</sup>M. L. Brewer, *J. Chem. Phys.* **111**, 6168 (1999).
- <sup>42</sup>E. J. Heller, *J. Chem. Phys.* **68**, 2066 (1978).
- <sup>43</sup>X. S. Sun and W. H. Miller, *J. Chem. Phys.* **117**, 5522 (2002).
- <sup>44</sup>Y. Elran and K. G. Kay, *J. Chem. Phys.* **110**, 3653 (1999).
- <sup>45</sup>A. R. Walton and D. E. Manolopoulos, *Mol. Phys.* **87**, 961 (1996).
- <sup>46</sup>H. Wang, D. E. Manolopoulos, and W. H. Miller, *J. Chem. Phys.* **115**, 6317 (2001).
- <sup>47</sup>M. D. Feit and J. A. Fleck, *J. Chem. Phys.* **78**, 301 (1983).
- <sup>48</sup>M. Nest and H. D. Meyer, *J. Chem. Phys.* **117**, 10499 (2002).
- <sup>49</sup>K. T. R. Davies, T. E. Huston, and M. Baranger, *Chaos* **2**, 215 (1992).
- <sup>50</sup>M. C. Gutzwiller, *J. Math. Phys.* **12**, 343 (1971).
- <sup>51</sup>M. Kús, F. Haake, and D. Delande, *Phys. Rev. Lett.* **71**, 2167 (1993).
- <sup>52</sup>T. Van Voorhis and D. R. Reichman *J. Chem. Phys.* (in press).